# Nonmonotonic polymer translocation kinetics through nanopores under changing surface–polymer interactions *⊗*

**Special Collection: Polymer Nanoconfinement** 

Neha Manohar 🗓 ; Robert A. Riggleman 🗷 🗓 ; Daeyeon Lee 🔽 🗓 ; Kathleen J. Stebe 🔀 🗓



J. Chem. Phys. 160, 084908 (2024) https://doi.org/10.1063/5.0189057











# Nonmonotonic polymer translocation kinetics through nanopores under changing surface-polymer interactions

Cite as: J. Chem. Phys. 160, 084908 (2024); doi: 10.1063/5.0189057 Submitted: 26 November 2023 • Accepted: 30 January 2024 • Published Online: 29 February 2024















## **AFFILIATIONS**

Department of Chemical and Biomolecular Engineering, University of Pennsylvania, Philadelphia, Pennsylvania 19104, USA

Note: This paper is part of the JCP Special Topic on Polymer Nanoconfinement.

<sup>a)</sup>Authors to whom correspondence should be addressed: rrig@seas.upenn.edu; daeyeon@seas.upenn.edu; and kstebe@seas.upenn.edu

#### **ABSTRACT**

Understanding the dynamics of polymers in confined environments is pivotal for diverse applications ranging from polymer upcycling to bioseparations. In this study, we develop an entropic barrier model using self-consistent field theory that considers the effect of attractive surface interactions, solvation, and confinement on polymer kinetics. In this model, we consider the translocation of a polymer from one cavity into a second cavity through a single-segment-width nanopore. We find that, for a polymer in a good solvent (i.e., excluded volume,  $u_0 > 0$ ), there is a nonmonotonic dependence of mean translocation time ( $\tau$ ) on surface interaction strength,  $\varepsilon$ . At low  $\varepsilon$ , excluded volume interactions lead to an energetic penalty and longer translocation times. As  $\varepsilon$  increases, the surface interactions counteract the energetic penalty imposed by excluded volume and the polymer translocates faster through the nanopore. However, as  $\varepsilon$  continues to increase, an adsorption transition occurs, which leads to significantly slower kinetics due to the penalty of desorption from the first cavity. The  $\varepsilon$ at which this adsorption transition occurs is a function of the excluded volume, with higher  $u_0$  leading to an adsorption transition at higher ε. Finally, we consider the effect of translocation across different size cavities. We find that the kinetics for translocation into a smaller cavity speeds up while translocation to a larger cavity slows down with increasing  $\varepsilon$  due to higher surface contact under stronger

Published under an exclusive license by AIP Publishing. https://doi.org/10.1063/5.0189057

#### I. INTRODUCTION

Macromolecular transport within confined spaces is fundamental to several biological, material, and environmental processes. The translocation of nucleic acids through porous biomembranes has major ramifications in DNA sequencing and processing, protein therapeutics, and drug delivery.2 It is essential to understand polymer transport kinetics in porous media for various applications, including heterogeneous catalyst development,3 membrane-based separations,<sup>4,5</sup> and enhanced oil recovery with polymeric flooding agents.<sup>6</sup> Despite significant efforts to study the mobility of macromolecules under confinement,<sup>7–16</sup> the combined influences of solvation, confinement, excluded volume and surface-polymer interactions on the kinetics of translocation are not well understood due to a complex interplay of thermodynamic parameters.6

We recently developed a method to fabricate polymer nanocomposite films with extremely high volume fractions of nanoparticles by infiltrating polymer into solvent-filled nanoparticle (NP) packings. This method not only facilitates the creation of nanocomposite films but also provides insight into the behavior of solvated polymers as they enter confined spaces, offering a deeper understanding of both kinetic and thermodynamic effects. Solventdriven Infiltration of Polymer (SIP) into NP packings involves solvent-vapor annealing of a bilayer composed of a densely packed NP layer atop an underlying polymer layer. In this process, solvent vapor undergoes capillary condensation within the NP packing and diffuses into the polymer film, initiating the infiltration of the solvated polymer into the interstitial voids of the NP packing.<sup>22</sup> The kinetics of the SIP process depend on the quality of solvent,<sup>22</sup> and the degree of confinement in the system. 18 The effect of polymer-NP interactions on infiltration during SIP has also been explored using molecular dynamics (MD) simulations.<sup>20</sup> By changing the Lennard-Jones (LJ) interaction energy between the polymer and the NP surface, three infiltration regimes were identified: (i) solvent-mediated infiltration in which polymer-NP interactions are very weak; (ii) surface-mediated infiltration driven by strong polymer-NP interactions; and (iii) an intermediate regime in which both solvation and surface interactions play a role.<sup>20</sup> This third regime emerges as a "goldilocks" regime with the fastest infiltration kinetics. These prior works motivate this current study, which aims to probe more deeply the kinetics of polymer translocation under confinement. This study is inspired by such previous work and seeks to extend our understanding of polymer translocation kinetics under confinement. Our streamlined model enables a comprehensive exploration across a wider spectrum of surface interaction strengths. Additionally, we are able to investigate the nuanced effects of solvent quality and confinement on translocation kinetics.

The entropic barrier model is a simple yet powerful methodology to understand how polymers overcome entropic barriers to move from one cavity to another. 23,24 The mean translocation time can be estimated by calculating the free energy of a polymer chain distributed between two connected cavities, with the connection being a single-segment width nanopore as illustrated in Fig. 1. This kinetic information is inferred from the free energy profile of the polymer as the number of segments between the two cavities is varied from zero to the total number of segments N.24,25 Previously, this model has been used to study an ideal polymer undergoing translocation through a pore in a planar membrane,25 out of a spherical vesicle,<sup>23</sup> between two cavities of different sizes, through an adsorbing hole,21 and through single-segment width channels of varying lengths.<sup>26</sup> This approach has also been used to study the transport of charged biomacromolecules through crowded environments<sup>27</sup> <sup>-29</sup> and has successfully modeled the behavior of polyelectrolytes translocating through a pore under an electric field gradient.<sup>29</sup> Polymer chains with excluded volume interactions require numerical analysis to address many body interactions. 19 One important factor that has yet to be addressed extensively is the impact of surface-polymer interactions on the translocation dynamics, specifically favorable interactions that can drive polymer adsorption to the surface. This aspect is particularly important in SIP because interactions between the polymer and the NP surface influence not only the dynamics of polymers filling the interstices of NP packings but also the mechanical properties of the resulting nanocomposite films.

In this study, translocation of a self-avoiding walk polymer between two circular cavities through a segment-width nanopore (entropic barrier) is considered (Fig. 1). We introduce and vary attractive interactions between the polymer chain and the inner surface of the cavities. We probe the effect of surface-polymer interactions on polymer translocation kinetics through the nanopore and investigate how this effect changes with solvent quality (excluded volume interactions) and confinement. The free energy landscape within the cavities is obtained from self-consistent field theory (SCFT) calculations, and these free energies are used to determine the mean translocation time  $(\tau)$  of the polymer from one cavity to the other through the nanopore using the Fokker-Planck equation. It is found that  $\tau$  strongly depends on the strength of the surface-polymer interactions and shows a non-monotonic dependence with surface interaction strength which qualitatively agrees with the MD simulations.<sup>20</sup> Furthermore, the "goldilocks" regime observed previously in the MD simulations is reproduced using this simple 2D model, where the effect of surface interaction and excluded volume complement each other, leading to fast translocation kinetics. Enhanced solvent quality (excluded volume interactions) extends this regime to higher surface interaction strengths. Finally, in the presence of strong surface interactions, higher confinement becomes more favorable, leading to faster translocation into spaces with greater confinement. These findings potentially provide guidelines on the fabrication of highly filled nanocomposites using SIP, the separation of macromolecules, and the design of catalytic supports for facilitating polymer upcycling reactions.

# II. METHODS

## A. Entropic barrier model to obtain $\tau$

In this model, a polymer chain escapes from cavity 1 to cavity 2 via a nanopore that is the width and length of a single polymer segment. The free energy of a polymer chain of N segments translocating can be calculated as a function of m, or the number of segments translocated into cavity 2. This free energy F(m) is found by

$$F(m) = F_1(N - m) + F_2(m), \tag{1}$$

where  $F_1(N-m)$  is the free energy of the portion of the chain of segment length (N-m) in cavity 1, and  $F_2(m)$  is the free energy of the

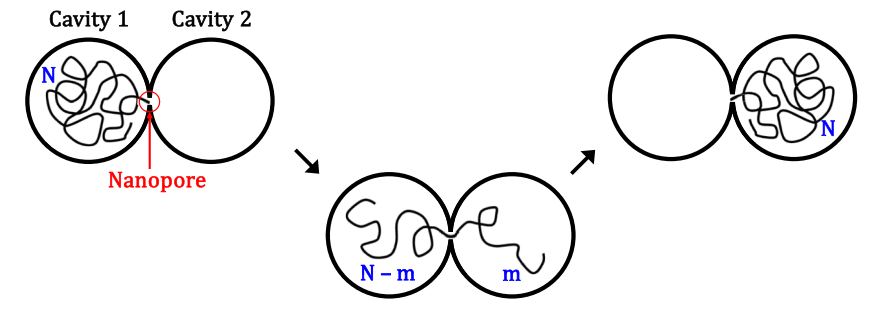


**FIG. 1.** Schematic illustration of polymer translocation in the entropic barrier model. *N* is the chain length of the polymer and *m* is the number of segments, which have translocated from the first cavity to the second cavity through a segment-width nanopore.

portion of the chain of segment length m in cavity 2. To obtain F(m) for any  $m = 1, 2, 3, \ldots, N$ , the free energy in each cavity as a function of chain length of polymer within that cavity must be calculated for chain lengths from 1 to N-1.

The mean translocation time  $(\tau)$  is defined as the average time for diffusion from a single segment translocated (m = 1) to all-but-one segment translocated (m = N - 1). This value is obtained by applying the adjoint Fokker–Planck operator to  $\tau$  and using the reflecting boundary condition at m = 0 and absorbing boundary condition at m = N, <sup>24,30</sup>

$$\tau = \frac{1}{k_0} \int_1^{N-1} dm \, e^{\beta F(m)} \int_1^m dm' \, e^{-\beta F(m')}. \tag{2}$$

Here,  $k_0$  is a rate constant associated with the translocation process. While our study provides important kinetic insights, a direct translation of these findings into physical timeframes for the SIP system is not feasible due to the distinct methodological and geometrical differences. There is also significant complexity in translating the mean translocation time obtained from the Fokker–Planck formalism, reported in this paper in units of  $1/k_0$ . This rate constant may be dependent on several factors, including but not limited to the frictional forces between the polymer segment and nanopore, the diffusivity of the polymer, as well as the surface interaction strength. To gain insights on the important trends, we normalize the mean translocation time by the translocation time for an ideal chain with no surface interactions.

### **B. SCFT simulations**

To find F(m) for the translocating polymer, a canonical model A (implicit solvent) homopolymer field theory in two dimensions is developed to obtain the partition function.<sup>31</sup> The effective potential between two polymer monomers in an implicit solvent can be expressed as the following simple delta function model:<sup>31</sup>

$$\overline{u}(r) = k_B T u_0 \delta(\mathbf{r}), \tag{3}$$

where  $u_0$  is the excluded volume interaction parameter.<sup>32</sup>

The Hubbard–Stratonovich particle-to-field transformation is employed to circumvent the many-body problem in the calculation of the partition function for a polymer system with excluded volume interactions, which transforms the partition function for the system into the field-theoretic form

$$Z = Z_0 \int D\omega \, \exp\left(-H[\omega(\mathbf{r})]\right). \tag{4}$$

In this equation, the partition function is shown as a functional integral over a chemical potential field  $\omega(\mathbf{r})$ , where  $H[\omega]$  is the effective Hamiltonian for a given field configuration. The prefactor,  $Z_0 \equiv (z_0 V)^n/n!$  is the partition function of an ideal gas of non-interacting polymers. The effective Hamiltonian for this system can be written as

$$H[\omega] = \frac{1}{2u_0} \int d\mathbf{r} [\omega(\mathbf{r})]^2 - n \ln Q[i\omega], \tag{5a}$$

$$Q[\omega] = \frac{1}{V} \int d\mathbf{r} \, q(\mathbf{r}, N; [\omega]). \tag{5b}$$

In this expression, Q is the normalized partition function, which can be calculated from the chain propagator  $q(\mathbf{r}, j; [\omega])$ , which is a functional for integer  $j = 0, 1, 2, \ldots, N-1$ , and represents the likelihood that the end of a chain with j+1 segments is located at  $\mathbf{r}$ . The initial condition for j+1=0 is defined as

$$q(\mathbf{r}, 0; [\omega]) = \exp[-\omega(\mathbf{r})]$$
 (6a)

and for  $j + 1 \neq 0$ ,

$$q(\mathbf{r},j+1;[w]) = \exp[-\omega(\mathbf{r})] \int d\mathbf{r}' \Phi(\mathbf{r} - \mathbf{r}') q(\mathbf{r}',j;[\omega]), \quad (6b)$$

where  $\Phi(r)$  is the normalized bond transition probability for a Gaussian chain. The initial condition of the chain propagator is modified to reflect being trapped in the entropic barrier at the inner surface of the cavity.

We take the mean-field approximation to calculate the effective Hamiltonian, where it is assumed that a single field configuration  $\omega^*(\mathbf{r})$  dominates. This field configuration can be obtained by imposing a stationary condition on the Hamiltonian to find saddle points, which for Model A can be written as

$$\frac{\delta H[\omega]}{\delta \omega(\mathbf{r})}\bigg|_{\omega=\omega^*} = \frac{1}{u_0}\omega^*(\mathbf{r}) + i\tilde{\rho}(\mathbf{r}, [i\omega^*]) = 0, \tag{7}$$

where  $\tilde{p}(r, [i\omega^*])$  is the segment density operator. The total number of statistical segments is equal to the volume integral of the segment density function. To find the saddle point, we use a continuous steepest descent relaxation method

$$\frac{\partial}{\partial t}\mu(\mathbf{r},t) = \lambda \frac{\delta H[\mu]}{\delta \mu(\mathbf{r},t)} = \lambda \left(-\frac{1}{u_0}\mu(\mathbf{r},t) + \tilde{\rho}(\mathbf{r};[\mu(t)])\right), \quad (8)$$

where  $\lambda > 0$  is a real relaxation parameter, and  $\mu(\mathbf{r},t) \equiv i\omega(\mathbf{r},t)$  is the real potential field. In Eq. (8), the time variable t represents a fictitious time corresponding to the update scheme for the fields and changes in the density as the field  $\mu(\mathbf{r},t)$  evolves do not correspond to physical dynamics.

To solve the above equation numerically, we discretize  $\mu(\mathbf{r},t)$  using a collocation method;  $\mu(\mathbf{r},t)$  and  $\tilde{\rho}(\mathbf{r};[\mu(t)])$  at M collocation points can be represented as vectors  $\mu(t)$  and  $\rho(\mu(t))$ , respectively, leading to a set of M nonlinear equations

$$\frac{d}{dt}\boldsymbol{\mu}(t) = -\frac{1}{u_0}\boldsymbol{\mu}(t) + \boldsymbol{\rho}(\boldsymbol{\mu}(t)). \tag{9}$$

We use a semi-implicit relaxation algorithm to solve this equation set following the method developed by Ceniceros and Frederickson.<sup>33</sup> The equation set can then be solved using a finite Fourier transform—inverse finite Fourier transform pair. The convergence criterion is set by calculating the error in the effective Hamiltonian between iterations, with a tolerance for convergence set at  $10^{-8}$ . To calculate the chain propagator, a pseudo-spectral scheme<sup>31</sup> for a bead–spring chain is propagated from the initial condition of j=0 to the chain end N-1. From here, the normalized partition function Q can be calculated and the free energy F obtained, as shown as follows:

$$F = \frac{F}{k_B T} \cong -\ln(Q). \tag{10}$$

The free energy calculated for a tethered chain ( $F_t$ ) is differentiated from the free energy of an untethered chain ( $F_{free}$ ) by adjusting the initial condition of the chain propagator to reflect the tethering condition [Eq. (6)].

# C. Integrated Lennard-Jones potential for surface interactions

To introduce surface interactions to the model, a wall density term is introduced. This term is applied when calculating the fields in each iteration of the SCFT code. To find the appropriate form of this term, a 12-6 Lennard-Jones (L-J) potential for a monomer or segment that is distance  $\rho$  from the center of the cavity, and r from the cavity wall (of radius R), is integrated over every point in the circular wall [Fig. S1(a)],

$$\varepsilon_{\text{shell}} = \int_{0}^{2\pi} d\theta \, n_{e} \left( 4\varepsilon \left[ \left( \frac{\sigma}{r} \right)^{12} - \left( \frac{\sigma}{r} \right)^{6} \right] \right) R.$$
(11)

Using the law of cosines to replace r with  $\rho$  and with  $a = \rho/R$ , the resulting form is given by

$$\begin{split} \epsilon_{shell,2D} &= 8\pi n_e \epsilon R \Bigg\{ \bigg( \frac{\sigma}{R} \bigg)^{12} \Bigg[ \frac{a^{10} + 25a^8 + 100a^6 + 100a^4 + 25a^2 + 1}{\big(a - 1\big)^{11} \big(a + 1\big)^{11}} \Bigg] \\ &- \bigg( \frac{\sigma}{R} \bigg)^6 \Bigg[ \frac{a^4 + 4a^2 + 1}{\big(a - 1\big)^5 \big(a + 1\big)^5} \Bigg] \Bigg\}. \end{split} \tag{12}$$

This potential is then integrated out over all possible wall radii to determine the interaction potential of the polymer with the particles in the wall beyond those on the wall surface

$$\varepsilon_{\text{wall}} = \int_{R_{\text{out}}}^{\infty} dR \, \varepsilon_{\text{shell}},$$
(13a)

$$\varepsilon_{\text{wall,2D}} = 4\pi n_{\text{e}} \varepsilon R^{2} \left\{ \left( \frac{\sigma}{R} \right)^{12} \left[ \frac{5a^{8} + 40a^{6} + 60a^{4} + 20a^{2} + 1}{5(1 - a)^{10}(1 + a)^{10}} \right] - \left( \frac{\sigma}{R} \right)^{6} \left[ \frac{2a^{2} + 1}{2(1 - a)^{4}(1 + a)^{4}} \right] \right\}.$$
(13b)

This equation is the final form of the cavity wall density and is implemented in the SCFT model by adding it to the field that is used to calculate the chain propagator.<sup>34</sup>

The resulting interactions with the cavity walls depend on the value of the surface interaction potential, defined here as  $\varepsilon \equiv \mathrm{n}_e \varepsilon$ , where  $\varepsilon$  is the L-J depth of the potential well. The surface interaction potential  $\varepsilon$  is varied from 0.001 to 0.05 to explore a full range of surface-polymer interactions. In our system, the L-J interaction length scale,  $\sigma$ , is equivalent to the length scale of the polymer segment (b), and both are taken to be unity. The cavity radius is therefore reported relative to the polymer segment length. In this system, a cavity radius R=5 represents a cavity with radius five times the length of a polymer segment.

#### III. RESULTS AND DISCUSSION

In Fig. 2, we calculate the change in free energy upon tethering the polymer chain end to the nanopore connecting cavity 1 to cavity 2,  $\Delta F_t$ . The free energy change, taken as

$$\Delta F_t = F_t(N) - F_{free}(N), \tag{14}$$

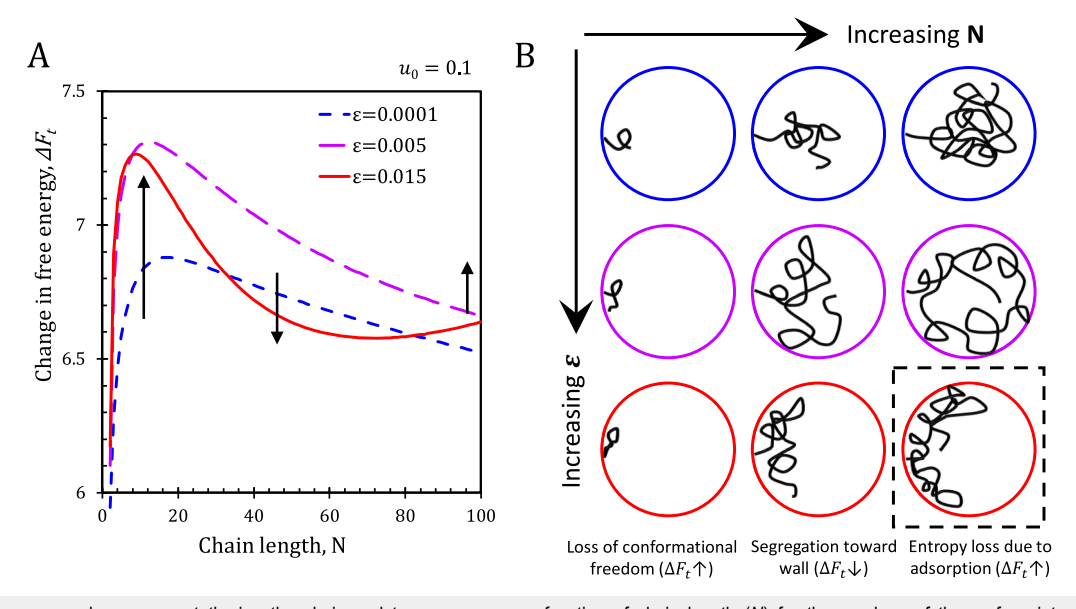


**FIG. 2.** (a) Free energy change upon tethering the chain end to nanopore as a function of chain length (N) for three values of the surface interaction parameter ( $\varepsilon = 0.0001, 0.005, 0.015$ ) in good solvent conditions ( $u_0 = 0.1$ ) in a confining cavity of size R = 5. (b) A schematic representation of the manner in which the chain length and surface interaction potential impact the free energy change upon tethering.

is plotted as a function of chain length, N, and is analyzed for low ( $\varepsilon$  = 0.0001), intermediate ( $\varepsilon$  = 0.005), and high ( $\varepsilon$  = 0.015) values of the surface interaction parameter between the polymer and the internal cavity surface; all energy scales are reported in units of  $k_BT$ .

The tethering-induced change in free energy  $(\Delta F_t)$  captures the impact of anchoring the chain end to the nanopore on the free energy of a polymer for a given N [Fig. S1(b)]. In the weak surface interaction case [Fig. 2(a), short blue dashed curve],  $\Delta F_t$ initially increases with increasing chain length, N, reflecting a loss in conformational entropy upon tethering. This effect is more pronounced in the cases of intermediate (purple long dashed curve) and strong (red solid curve) surface interaction and can be attributed primarily to polymer adsorption on the cavity surface. As N continues to increase,  $\Delta F_t$  goes through a maximum. The subsequent reduction in  $\Delta F_t$  for increasing N is attributed to increased pressure from excluded volume interactions, which lead the self-avoiding walk polymer to organize closer to the cavity surface, thereby facilitating the polymer chain ends' ability to more readily access the nanopore. This behavior is consistent with prior studies on entropic barriers that account for excluded volume effects. 19 However, in the case of strong surface interaction [Fig. 2(a), red solid], this decrease in  $\Delta F_t$  reverses at higher values of N. This trend is attributed to a steep loss of conformational entropy upon polymer adsorption on the cavity surface, which is especially significant for longer chains. As the surface-polymer interaction becomes stronger, the radially averaged segment density profiles shift from being primarily located in the cavity's center and away from the surface to clustering near the surface (Fig. S2). This shift indicates strong polymer affinity to the cavity surface, which becomes more entropically challenging to satisfy with increasing N when one chain end is tethered.

These competing effects influence the kinetics of polymer translocation through the nanopore by altering the free energy landscape. In Fig. 3(a), the free energy profile of the polymer chain, F(m), as it translocates through the nanopore from cavity 1  $(R_1 = 5)$  to cavity 2 ( $R_2 = 5$ ) is shown for the three surface interaction cases [calculated using Eq. (1)]. For the case with weak interaction strength  $\varepsilon$  = 0.0001 (Fig. 3, blue), there is a free energy minimum at m = 50. This minimum can be attributed to the excluded volume effect;<sup>19</sup> the polymer chain is able to occupy the largest volume by spreading itself equally between the volume of two cavities. This free energy minimum slows the second half of the translocation process since each additional translocated segment for m > 50 increases the crowding of the self-avoiding walk polymer in the second cavity. In contrast, the free energy profile for the strongly interacting case  $\varepsilon = 0.015$ (Fig. 3, red) exhibits a maximum at m = 50. In this case, highly favorable surface contact is maximized when the longest possible chain length is present within a single cavity, leading to very low free energies at the beginning and end of the translocation profile (m = 0or m = 100). This implies that spreading of the self-avoiding polymer between the surfaces of the two cavities induces a free energy penalty. This maximum in the free energy represents a significant energy barrier to polymer translocation, leading to longer translocation kinetics. Interestingly, the intermediate interaction case with  $\varepsilon$ = 0.005 (Fig. 3, purple) has a relatively featureless free energy profile with no significant energy barrier as the excluded volume effect is offset by the adsorption effect, essentially creating a "goldilocks" regime where translocation is not impeded by either mechanism and therefore translocation occurs the fastest.

These trends in the free energy profile result in a nonmonotonic dependence of normalized mean translocation time,  $\tau/\tau_0$ , with increasing surface interaction strength, as shown in Fig. 4. The mean translocation time is normalized by  $\tau_0$ , which is defined as the

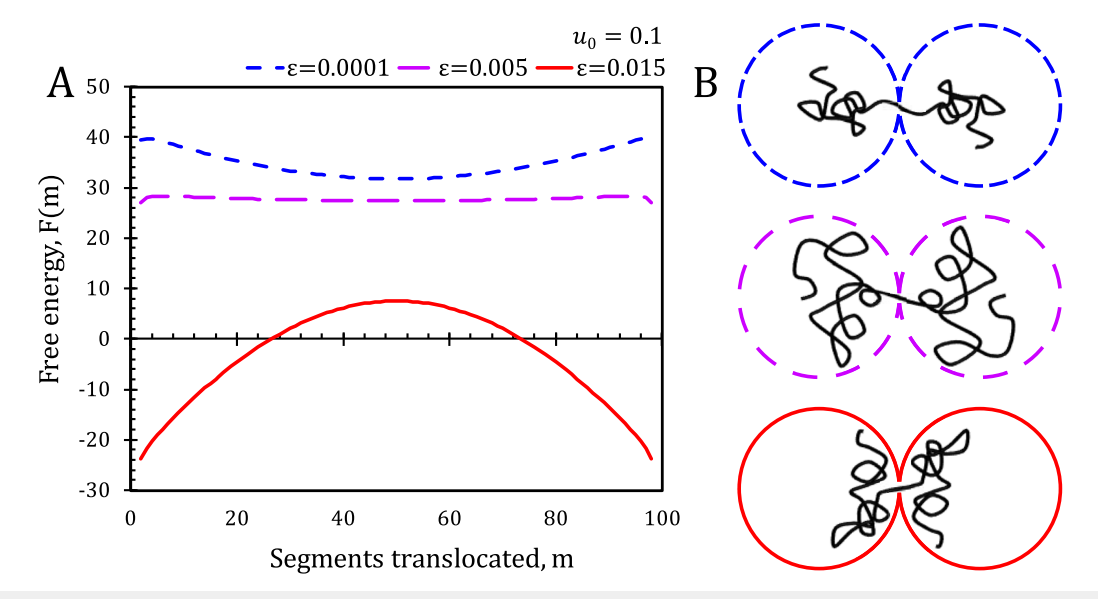


**FIG. 3**. Free energy profile for translocation of a polymer chain with N=100 between cavities of radius R=5. (a) For excluded volume interaction  $u_0=0.1$ , translocating from cavity 1 to cavity 2 with weak ( $\varepsilon=0.0001$ , blue), intermediate ( $\varepsilon=0.005$ , purple), and strong ( $\varepsilon=0.015$ , red) surface interactions between the polymer and cavity surface. (b) Schematic illustration of three surface-interaction cases.

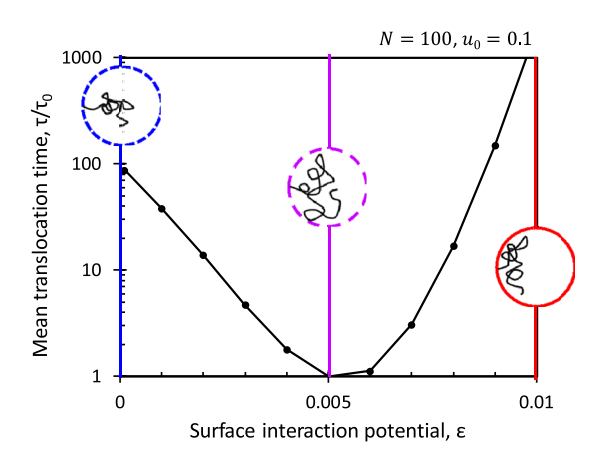


**FIG. 4.** The normalized mean translocation time,  $\tau/\tau_0$ , of a polymer chain of length N=100 with excluded volume parameter  $u_0=0.1$  as a function of surface interaction potential,  $\varepsilon$ .

time for an ideal chain ( $u_0 = 0$ ) with very weak surface interaction ( $\varepsilon = 0.0001$ ) to translocate from cavity 1 to cavity 2. For weak surface interaction strengths ( $\varepsilon < 0.005$ ),  $\tau/\tau_0$  decreases with increasing  $\varepsilon$  since the magnitude of the free energy barrier decreases (Fig. 4) with increasing interaction strength.

However, for higher surface interactions ( $\varepsilon > 0.005$ ),  $\tau/\tau_0$  increases significantly as polymer adsorbs on the cavity surface. The magnitude of the free energy maximum at m=50 increases with increasing  $\varepsilon$ , leading to significantly slower translocation of the polymer from cavity 1 to cavity 2.

The effect of excluded volume on this phenomenon is further explored by considering a range of  $u_0$  values (Table I), which cover the range from a theta (poor) solvent ( $u_0 = 0, \chi = 0.5$ ) to a very good solvent ( $u_0 = 0.5, \chi = 0.25$ ). Here, the Flory–Hugging  $\chi$  parameter is obtained from the excluded volume using the following relation, where  $v_0$  is the monomer volume:

$$u_0 = v_0(1 - 2\chi). \tag{15}$$

When the excluded volume parameter is increased and the quality of the implicit solvent improves, the polymer expands and occupies the space within the cavity more uniformly, as is evident in the expansion of the density curves in Figs. S3 and S4. We find

**TABLE I.** The values of the Flory–Huggins  $\chi$  parameter and the radius of gyration  $(R_g)$  for a polymer chain with N=100 in a cavity of radius R=5 at five values of the excluded volume parameter.

Excluded volume, $u_0 (b^3)$	Flory–Huggins $\chi$ parameter	Radius of gyration, $R_g(b)$
0 <sup>a</sup>	0.50	4.08
0.03	0.49	4.08
0.1	0.45	4.08
0.3	0.35	5.09
0.5	0.25	5.63

 $<sup>^{</sup>a}R_{g}$  for  $u_{0}$  < 0.1 calculated using ideal scaling; for  $u_{0}$  ≥ 0.1 calculated using good solvent scaling (see the supplementary material).

that these density shifts are comparable to those reported by Kong and Muthukumar<sup>19</sup> upon increasing excluded volume interactions in their three-dimensional entropic barrier model, which did not have any surface interactions between the polymer and cavity surface (Fig. S4). This behavior is attributed to the penalty imposed by the excluded volume on crowding of polymer in the center of the cavity or at the inner surface of the cavity, effectively dampening the effect of surface interactions on polymer density.

This competition between excluded volume and surface interaction strength is also apparent in the behavior of  $\tau/\tau_0$  with respect to the surface interaction parameter,  $\varepsilon$  (Fig. 5). With no excluded volume ( $u_0 = 0$ ), there is monotonic dependence of  $\tau/\tau_0$  with  $\varepsilon$ (Fig. 5, black solid curve); the surface interaction causes  $\tau/\tau_0$  to increase with  $\varepsilon$  as the increasing energy barrier for polymer desorption from the walls of the first cavity impedes the rate of translocation into the second cavity. Even at the smallest excluded volume parameter ( $u_0 = 0.03$ , dark grey long dashed curve in Fig. 5), however, we observe nonmonotonic behavior. By introducing excluded volume effects, a local minimum appears in the translocation free energy profile, leading to elevated  $\tau/\tau_0$  values even for weak  $\varepsilon$ . As the excluded volume parameter increases (Fig. 5, grey curves), a specific  $\varepsilon$  value emerges for which the free energy profile flattens, indicating that adsorption effects counteract the excluded volume effects, as shown in Fig. 3. For this value of  $u_0$  and  $\varepsilon$ ,  $\tau/\tau_0 = 1$  and the translocation rate is at its most rapid, occurring at the same speed as that for an ideal chain with very low surface-polymer interactions. This phenomenon indicates that increasing excluded volume effects shift the adsorption transition for which polymer crowds close to the pore walls to progressively higher  $\varepsilon$  values where the better solvent (larger  $u_0$ ) requires stronger adsorption for the polymer to give up its favorable polymer-solvent contacts and adopt a compact shape near the wall.

To validate this observation, we calculate the adsorption transition using density profiles. Figure 6(a) shows the average distance of the polymer from the center of the cavity, calculated from the tethered polymer density profiles, plotted against  $\epsilon$ . By fitting a

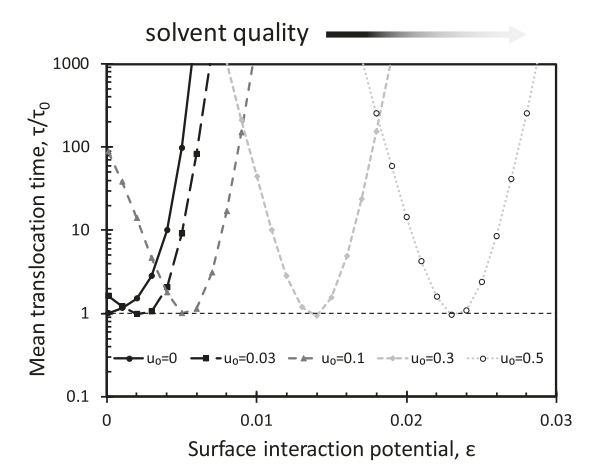


**FIG. 5.** The normalized mean translocation time,  $\tau/\tau_0$ , of a polymer chain of length N=100 as a function of surface interaction potential,  $\varepsilon$ , for various values of the excluded volume parameter  $u_0$ .

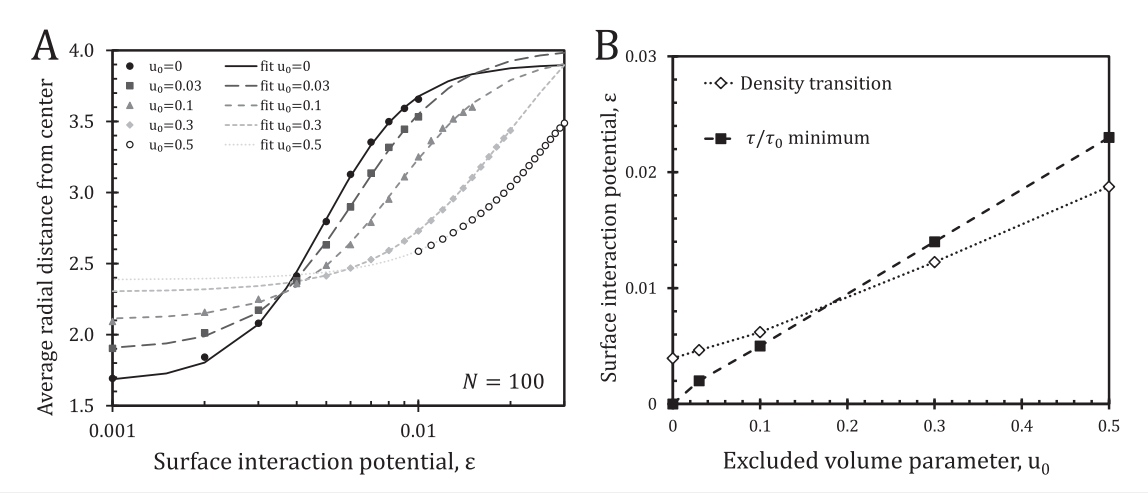


**FIG. 6.** (a) The average radial distance from the center of the cavity of a tethered polymer (*N* = 100) as a function of surface interaction potential for five values of excluded volume (markers) along with a fitted curve (grayscale lines). (b) The adsorption transition calculated from the fitted inflection points from the average polymer densities (open diamonds, dotted line) and the surface interaction potential at which the minimum in mean translocation time occurs (solid squares, dashed line) as a function of the excluded volume parameter. Lines are to guide the eye.

hyperbolic tangent curve to the data, the interaction strength corresponding to the adsorption transition can be identified through the inflection point. In Fig. 6(b), this inflection point from the hyperbolic tangent fit is plotted against  $u_0$  to examine the influence of excluded volume on the adsorption transition (open diamond) and is compared against the  $\varepsilon$  value at which the mean translocation time reaches its minimum where  $\tau/\tau_0=1$  (solid square). The two curves have similar values for the adsorption transition; however, the values based on the minima in the  $\tau/\tau_0$  curves have a steeper slope, indicating a stronger dependence on the excluded volume parameter. This difference in slope could imply that certain excluded volume effects are not fully captured by the density profiles, or it may stem from the fitting methodology used in Fig. 6(a).

Next, we explore the kinetics when the two confining cavities differ in size, focusing on how increasing surface interactions alter translocation kinetics. Absent surface interactions or excluded volume effects (i.e., an ideal chain), the polymer translocates more quickly into larger and more slowly into smaller cavities, consistent with prior studies. Entering a smaller cavity requires the polymer to sacrifice conformational entropy, manifesting as a higher free energy barrier for the process. The introduction of excluded volume effects amplifies this trend, resulting in slower entry into smaller cavities and faster entry into larger cavities compared to the behavior of an ideal chain. <sup>19</sup>

We now consider how surface interactions influence this process. The kinetics of infiltration from a small cavity  $(R_1 = 5)$  to a larger cavity  $(R_2 = 10)$  for an excluded volume of  $u_0 = 0.1$  is shown in Fig. 7(a) (yellow triangles). We find that  $\tau/\tau_0$  increases monotonically with increasing  $\varepsilon$ . At low  $\varepsilon$ , translocation from a small to a large cavity occurs more rapidly than ideal chain translocation between identical cavities, i.e.,  $\tau < \tau_0$ . This behavior differs from the symmetric case  $[R_1 = R_2 = 5, \text{ Fig. 7(a)}, \text{ black circles}], \text{ reproduced from Fig. 5, for which the kinetics is nonmonotonic with$ 

respect to  $\varepsilon$  and bounded below by the ideal chain translation time.

This accelerated translocation from small to large cavity is attributed to the significant entropic gain as the polymer enters the larger cavity. This reduced confinement results in a negative slope in the free energy profile, which is distinct from the symmetric case which cannot have an asymmetric free energy profile (Fig. S5). At higher surface interaction strengths ( $\varepsilon$  > 0.007), this rapid translocation regime ends, and  $\tau$  becomes larger than  $\tau_0$  as adsorption in cavity 1 becomes the dominant factor. At these higher interaction strengths, the polymer can adsorb more readily in the smaller cavity 1 than in the larger cavity 2, reversing the slope of the free energy profile and significantly slowing down the translocation kinetics into the larger cavity.

We also consider the case of increasing confinement, for which the polymer translocates from a larger cavity ( $R_1 = 10$ ) into a smaller one  $(R_2 = 5)$ , as shown in the bottom schematic in Fig. 7(b). Here,  $\tau/\tau_0$  also changes monotonically with surface interaction strength [Fig. 7(a), green squares]. However, the trend is reversed; the kinetics accelerate with increasing  $\varepsilon$ . At low surface interaction strengths,  $\tau/\tau_0$  is significantly higher than the cases for equal sized cavities of reduced confinement upon translocation; the increased confinement in cavity 2 incurs a substantial entropic penalty upon translocation. However,  $\tau/\tau_0$  sharply decreases with increasing  $\varepsilon$  because the larger cavity 1 offers fewer opportunities for polymer adsorption, whereas the smaller cavity 2 facilitates polymer adsorption. Uniquely in this case, increasing surface interaction does not eventually result in a steep rise in  $\tau/\tau_0$ . Rather,  $\tau$  falls below  $\tau_0$  at the highest  $\varepsilon$  values considered. The observed behavior can again be attributed to a negative slope of the translocation free energy profile, as high surface interaction strengths make it energetically favorable for the polymer to reside in the smaller cavity. This finding has intriguing implications for polymer infiltration in highly confined systems and suggests that

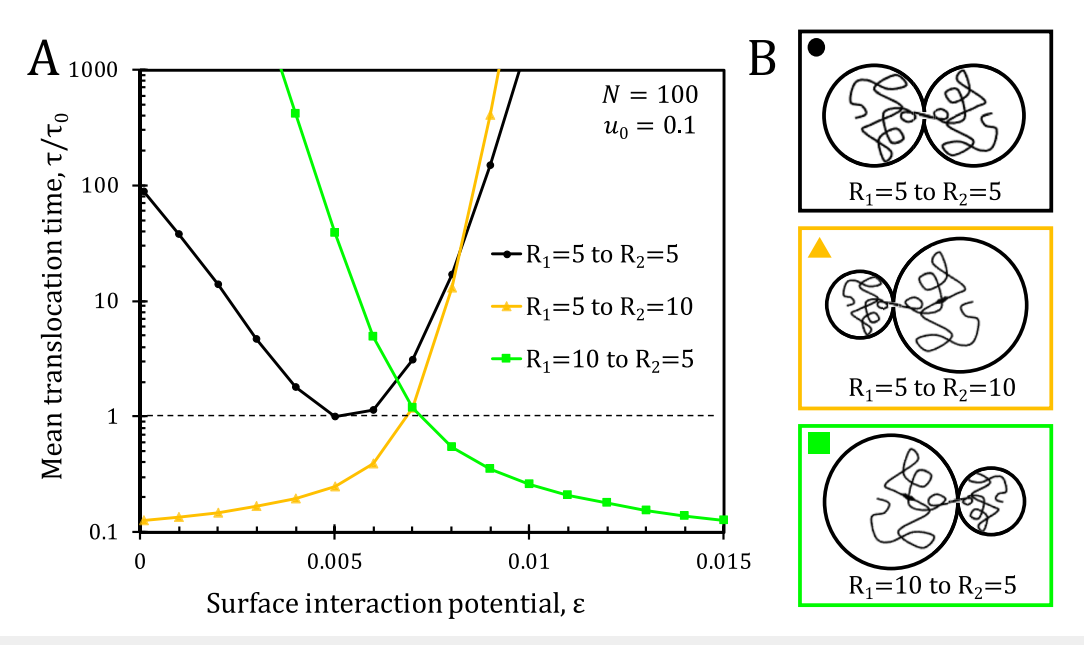


**FIG. 7.** (a) The normalized mean translocation time,  $\tau/\tau_0$ , of a polymer chain of length N=100 with excluded volume parameter  $u_0=0.1$  as a function of surface interaction potential,  $\varepsilon$ , for translocation from a cavity of  $R_1=5$  to another of  $R_2=5$  (black circles), translocation from a cavity of  $R_1=10$  to one of  $R_2=10$  (yellow triangles) and translocation from a cavity of  $R_1=10$  to one of  $R_2=10$  (yellow triangles). (b) Schematic representation of each translocation case.

by designing a system with strong interactions between the polymer and the confining surface, polymer infiltration into even extremely confined geometries can be facilitated.

#### IV. CONCLUSIONS

In this work, we have studied the effect of surface-polymer interactions, solvent quality, and confinement on the kinetics of polymer translocation between two circular cavities through a single segment-width nanopore. Using the entropic barrier model, we have identified a "goldilocks" regime where surface interactions and excluded volume effects synergize for the fastest translocation kinetics. As the quality of the solvent improves, the optimal strength of surface-polymer interactions for the fastest translocation kinetics increases since better solvent quality shifts the adsorption transition to higher surface-polymer interaction strengths. Additionally, our results reveal how varying cavity sizes impact translocation kinetics. Translocation from a smaller to a larger cavity is facilitated by weakening surface-polymer interaction due to entropic gains. Conversely, a polymer that moves from a larger to a smaller cavity has faster translocation kinetics for stronger surface interactions, a counterintuitive result that could facilitate polymer infiltration into highly confined systems. We note that the results presented herein assume that the friction between the monomers will not appreciably change during adsorption to the pore wall; it is wellknown that strong adsorption can lead to a significant reduction in the dynamics of polymers near a wall, 35,36 which may further increase the translocation time at large  $\varepsilon$ . Our results provide important insights and guidance in fabricating nanocomposite films via SIP and designing catalytic supports or separation membranes to

facilitate polymer transport and thus eliminate possible transport limitations.

# SUPPLEMENTARY MATERIAL

See the supplementary material for the following: details regarding the radius of gyration ( $R_g$ ) calculations; schematics of the coordinate system used to analyze bead interactions within the cavity; schematics of tethered vs free chains; details concerning the untethered chain-surface interactions; untethered chain response to solvent quality and tethered chain response to excluded volume; and details regarding free energy profiles for chains translocating between different sized cavities.

# **ACKNOWLEDGMENTS**

This work was supported by the National Science Foundation (NSF; Grant Nos. NSF CBET-1933704 and NSF CBET-1945841).

# **AUTHOR DECLARATIONS**

#### Conflict of Interest

The authors have no conflicts to disclose.

#### **Author Contributions**

**Neha Manohar**: Conceptualization (equal); Data curation (equal); Formal analysis (equal); Investigation (equal); Methodology (equal);

Validation (equal); Visualization (equal); Writing - original draft (equal); Writing - review & editing (equal). Robert A. Riggleman: Conceptualization (equal); Formal analysis (equal); Investigation (equal); Methodology (equal); Software (equal); Supervision (equal); Writing - review & editing (equal). Daeyeon Lee: Conceptualization (equal); Funding acquisition (equal); Investigation (equal); Methodology (equal); Supervision (equal); Validation (equal); Writing original draft (equal); Writing - review & editing (equal). Kathleen J. Stebe: Conceptualization (equal); Supervision (equal); Writing – original draft (equal); Writing - review & editing (equal).

#### **DATA AVAILABILITY**

The data that support the findings of this study are available within the article and its supplementary material.

#### **REFERENCES**

- <sup>1</sup>D. Deamer, M. Akeson, and D. Branton, "Three decades of nanopore sequencing," Nat. Biotechnol. 34(5), 518-524 (2016).
- <sup>2</sup>Y. Huang, L. Liu, C. Luo, W. Liu, X. Lou, L. Jiang, and F. Xia, "Solid-state nanochannels for bio-marker analysis," Chem. Soc. Rev. 52(18), 6270-6293
- <sup>3</sup>Q. Sun, Z. Dai, X. Meng, and F.-S. Xiao, "Porous polymer catalysts with hierarchical structures," Chem. Soc. Rev. 44(17), 6018-6034 (2015).
- <sup>4</sup>M. Farrokhnia, A. Safekordi, M. Rashidzadeh, G. Khanbabaei, R. Akbari Anari, and M. Rahimpour, "Development of porous nanocomposite membranes for gas separation by identifying the effective fabrication parameters with Plackett-Burman experimental design," J. Porous Mater. 23(5), 1279-1295 (2016). <sup>5</sup>B.-H. Jeong, E. M. V. Hoek, Y. Yan, A. Subramani, X. Huang, G. Hurwitz, A. K. Ghosh, and A. Jawor, "Interfacial polymerization of thin film nanocomposites: A new concept for reverse osmosis membranes," J. Membr. Sci. 294(1-2), 1-7
- <sup>6</sup>H. Chen and M. E. Poitzsch, "Dynamics of polymers flowing through porous media: Interplay of solvent properties, flow rates, and wetting," Macromolecules 55(24), 11068-11075 (2022).
- <sup>7</sup>M. D. Ediger and J. A. Forrest, "Dynamics near free surfaces and the glass transition in thin polymer films: A view to the future," Macromolecules 47(2), 471-478
- <sup>8</sup>B. Frank, A. P. Gast, T. P. Russell, H. R. Brown, and C. Hawker, "Polymer mobility in thin films," Macromolecules 29(20), 6531-6534 (1996).
- <sup>9</sup>K. Chrissopoulou and S. H. Anastasiadis, "Effects of nanoscopic-confinement on polymer dynamics," Soft Matter 11(19), 3746–3766 (2015). <sup>10</sup>C.-C. Lin, S. Gam, J. S. Meth, N. Clarke, K. I. Winey, and R. J. Composto,
- "Do attractive polymer-nanoparticle interactions retard polymer diffusion in nanocomposites?," Macromolecules 46(11), 4502-4509 (2013).
- <sup>11</sup>S. Jin and G. B. McKenna, "Effect of nanoconfinement on polymer chain dynamics," Macromolecules 53(22), 10212-10216 (2020).
- <sup>12</sup>R. Kimmich, N. Fatkullin, C. Mattea, and E. Fischer, "Polymer chain dynamics under nanoscopic confinements," Magn. Reson. Imaging 23(2), 191-196 (2004).
- <sup>13</sup>D. Richter and M. Kruteva, "Polymer dynamics under confinement," Soft Matter 15(37), 7316-7349 (2019).
- $^{14}\mathrm{M}.$  T. Bishop, K. H. Langley, and F. E. Karasz, "Dynamic light-scattering studies of polymer diffusion in porous materials: Linear polystyrene in porous glass," Macromolecules 22(3), 1220-1231 (1989).

- 15 J. L. Hor, H. Wang, Z. Fakhraai, and D. Lee, "Effects of polymer-nanoparticle interactions on the viscosity of unentangled polymers under extreme nanoconfinement during capillary rise infiltration," Soft Matter 14(13), 2438-2446
- 16 J. L. Hor, H. Wang, Z. Fakhraai, and D. Lee, "Effect of physical nanoconfinement on the viscosity of unentangled polymers during capillary rise infiltration," Macromolecules 51(14), 5069-5078 (2018).
- <sup>17</sup>M. Muthukumar, "Entropic barrier model for polymer diffusion in concentrated polymer solutions and random media," J. Non-Cryst. Solids 131-133, 654-666 (1991).
- <sup>18</sup>N. Manohar, K. J. Stebe, and D. Lee, "Effect of confinement on solvent-driven infiltration of the polymer into nanoparticle packings," Macromolecules 53(15), 6740-6746 (2020).
- <sup>19</sup>C. Y. Kong and M. Muthukumar, "Polymer translocation through a nanopore. II. Excluded volume effect," J. Chem. Phys. 120(7), 3460-3466 (2004).
- <sup>20</sup>R. B. Venkatesh, T. Zhang, N. Manohar, K. J. Stebe, R. A. Riggleman, and D. Lee, "Effect of polymer-nanoparticle interactions on solvent-driven infiltration of polymer (SIP) into nanoparticle packings: A molecular dynamics study," Mol. Syst. Des. Eng. 5(3), 666–674 (2020).
- 21 P. J. Park and W. Sung, "Polymer translocation induced by adsorption," J. Chem. Phys. 108(7), 3013-3018 (1998).
- <sup>22</sup>N. Manohar, K. J. Stebe, and D. Lee, "Solvent-driven infiltration of polymer (SIP) into nanoparticle packings," ACS Macro Lett. 6(10), 1104-1108
- <sup>23</sup>P. J. Park and W. Sung, "Polymer release out of a spherical vesicle through a pore," Phys. Rev. E 57(1), 730–734 (1998).

  <sup>24</sup>M. Muthukumar, "Polymer translocation through a hole," J. Chem. Phys.
- 111(22), 10371-10374 (1999).
- 25 W. Sung and P. J. Park, "Polymer translocation through a pore in a membrane," Phys. Rev. Lett. 77(4), 783-786 (1996).
- <sup>26</sup>M. Muthukumar, "Polymer escape through a nanopore," J. Chem. Phys. 118(11), 5174-5184 (2003).
- <sup>27</sup>K. Chen and M. Muthukumar, "Entropic barrier of topologically immobilized DNA in hydrogels," Proc. Natl. Acad. Sci. U. S. A. 118(28), e2106380118 (2021).
- <sup>28</sup>R. Kumar and M. Muthukumar, "Origin of translocation barriers for polyelectrolyte chains," J. Chem. Phys. 131(19), 194903 (2009).
- <sup>29</sup>B. Cressiot, A. Oukhaled, G. Patriarche, M. Pastoriza-Gallego, J.-M. Betton, L. Auvray, M. Muthukumar, L. Bacri, and J. Pelta, "Protein transport through a narrow solid-state nanopore at high voltage: Experiments and theory," ACS Nano **6**(7), 6236–6243 (2012).
- <sup>30</sup>H. Risken, The Fokker-Planck Equation: Methods of Solution and Applications, Springer Series in Synergetics (Springer, Berlin, Heidelberg, 2011), pp. 63-95.
- <sup>31</sup>G. H. Fredrickson, The Equilibrium Theory of Inhomogeneous Polymers (Oxford University Press, 2005).
- 32 S. F. Edwards, "The statistical mechanics of polymers with excluded volume," Proc. Phys. Soc. 85(4), 613-624 (1965).
- 33 H. D. Ceniceros and G. H. Fredrickson, "Numerical solution of polymer selfconsistent field theory," Multiscale Model. Simul. 2(3), 452-474 (2004).
- <sup>34</sup>M. W. Matsen, "Thin films of block copolymer," J. Chem. Phys. 106(18), 7781-7791 (1997).
- $^{\bf 35}{\rm M.\,F.\,Thees}$  , J. A. McGuire, and C. B. Roth, "Review and reproducibility of forming adsorbed layers from solvent washing of melt annealed films," Soft Matter 16(23), 5366-5387 (2020).
- <sup>36</sup>M. J. Burroughs, S. Napolitano, D. Cangialosi, and R. D. Priestley, "Direct measurement of glass transition temperature in exposed and buried adsorbed polymer nanolayers," Macromolecules 49(12), 4647-4655 (2016).